the FEBS Journal

The reactive oxygen species–Src–Stat3 pathway provokes negative feedback inhibition of apoptosis induced by high-fluence low-power laser irradiation

Xuegang Sun, Shengnan Wu and Da Xing

MOE Key Laboratory of Laser Life Science & Institute of Laser Life Science, College of Biophotonics, South China Normal University, Guangzhou, China

Keywords
high-fluence low-power laser irradiation; negative feedback inhibition; reactive oxygen species (ROS); Src; Stat3

Correspondence
D. Xing, MOE Key Laboratory of Laser Life Science & Institute of Laser Life Science, College of Biophotonics, South China Normal University, Guangzhou 510631, China
Fax: +86 20 85216052
Tel: +86 20 85211438; Ext. 8303
E-mail: xingda@scnu.edu.cn

(Received 12 May 2010, revised 31 August 2010, accepted 14 September 2010)

doi:10.1111/j.1742-4658.2010.07884.x

High-fluence low-power laser irradiation (HF-LPLI) can induce apoptosis by triggering mitochondrial oxidative stress. Signal transducer and activator of transcription 3 (Stat3) is an important transcription factor in the modulation of cell proliferation and apoptosis. Here, using real-time single-cell analysis and western blotting analysis, we investigated the changes in activities of Stat3 in COS-7 cells upon HF-LPLI (633 nm, 80 and 120 J·cm^{-2}) and the underlying mechanisms involved. We found that Stat3 was significantly activated by HF-LPLI in a time-dependent and dose-dependent manner. Stat3 activation attenuated HF-LPLI-induced apoptosis, as shown by the fact that both dominant negative Stat3 (Y705F) and Stat3 small interfering RNA expression enhanced cellular apoptosis induced by HF-LPLI. Moreover, we also found that Src kinase was the major positive regulator of Stat3 activation induced by HF-LPLI. Reactive oxygen species (ROS) generation was essential for Stat3 and Src activation upon HF-LPLI, because scavenging of ROS by vitamin C or *N*-acetylcysteine totally abrogated the activation of Stat3 and Src. Taken together, these findings show that the ROS–Src–Stat3 pathway mediates a negative feedback inhibition of apoptosis induced by HF-LPLI in COS-7 cells. Our research will provide new insights into the mechanism of apoptosis caused by HF-LPLI, and also extend the functional study of Stat3.

Introduction

High-fluence low-power laser irradiation (HF-LPLI) is a newly discovered stimulator, and can activate intrinsic mitochondrial apoptosis pathway. HF-LPLI has been reported to interfere with cell cycling and inhibit cell proliferation [1–3]. In 2005, Wang *et al.* [4] reported that HF-LPLI can induce cell apoptosis by activating caspase-3 in human lung adenocarcinoma cells (ASTC-a-1). In 2007, Wu *et al.* [5,6] report that mitochondrial permeability transition is the main mechanism of mitochondrial injury on stimulation with HF-LPLI, thus resulting in outer mitochondrial membrane permeabilization. Bax activation is a downstream event of HF-LPLI-induced apoptosis [6]. Notably, the dominant factor in HF-LPLI-induced apoptosis is

Abbreviations
CFP, cyan fluorescent protein; DCF, dichlorofluorescein; DN, dominant negative; EGF, epidermal growth factor; FITC, fluorescein isothiocyanate; FRET, fluorescence resonance energy transfer; H_2DCFDA, 2′,7′-dichlorodihydrofluorescein diacetate; HF-LPLI, high-fluence low-power laser irradiation; IL-6, interleukin-6; JAK, janus kinase; NAC, *N*-acetylcysteine; PI, propidium iodide; PP1, 4-amino-5-(4-methylphenyl)-7-(t-butyl) pyrazolo(3,4-d)-pyrimidine; PTP, protein tyrosine phosphatase; ROS, reactive oxygen species; SEM, standard error of the mean; siRNA, small interfering RNA; Stat3, signal transducer and activator of transcription 3; STS, staurosporine; YFP, yellow fluorescent protein.

the large and toxic dose of reactive oxygen species (ROS) generated through selective activation of endogenous photoacceptors by 633 nm laser irradiation [6]. However, the mechanism associated with the stimulatory effects of HF-LPLI has not been fully clarified.

Signal transducer and activator of transcription 3 (Stat3) is an important transcription factor that participates in a wide variety of physiological processes, such as cell proliferation, survival, differentiation and apoptosis [7,8]. Stat3 is ubiquitously expressed, and is activated by a number of receptor and nonreceptor tyrosine kinases [7,9]. Phosphorylation of Stat3 at Tyr705 is necessary for Stat3 activation. Phosphorylated Stat3 translocates to the nucleus, binds to the specific promoters of target genes, and induces gene expression [8,9].

Our previous work has shown that HF-LPLI induces ROS generation [6]. ROS are reported to be ubiquitous, highly diffusable and reactive molecules that are known as important secondary messengers and are supposed to play key roles in light–tissue interactions [10,11]. In the past few years, there has been increasing recognition of their role as redox regulators of cellular signaling [12]. ROS have been shown to mediate Stat3 signaling in addition to growth factors and cytokines [13]. Therefore, the aim of this study was to explore the involvement of Stat3 in the regulation of apoptosis induced by HF-LPLI.

Both Src kinases and janus kinases (JAKs) have been reported to mediate Stat3 activation following cytokine/growth factor stimulation [7,14]. ROS are traditional stimulators for inducing the activation of Stat3 involving Src and JAKs [13,15]. Furthermore, work by Zhang *et al*. [16] showed the activation of Src by ROS generation induced by HF-LPLI at relatively high laser doses (25 and 50 $J{\cdot}cm^{-2}$). Thus, it is rational to speculate that Src may be involved in Stat3 activation under HF-LPLI.

Determining the mechanisms of HF-LPLI will be of benefit for the clinical application of low-power laser therapies. It can also be used to treat some types of hyperplasia [1–3], and to treat cancers, like the usage of photodynamic treatment [17] in the absence of photosensitizers. Finally, HF-LPLI represents a new stimulator to trigger cell apoptosis, and could be used widely as a new and low-cost method to induce cellular apoptosis for research and therapy.

The overall objective of the present study was to define the role of Stat3 in HF-LPLI-induced apoptosis, and to discuss the activation mechanisms involved. We demonstrated that the ROS–Src–Stat3 signaling pathway was activated by HF-LPLI, and that this pathway activation could, in turn, inhibit HF-LPLI-induced apoptosis; this is a typical process of negative feedback inhibition.

Results

Stat3 is activated by HF-LPLI in a time-dependent and dose-dependent manner

To monitor the changes in the subcellular localization of Stat3 under HF-LPLI, cells were transfected with Stat3–yellow fluorescent protein (YFP). After 48 h of expression, the dynamics of Stat3–YFP in positive transfected cells were monitored by confocal microscopy. We found that Stat3 was mainly localized in the cytoplasm in cells with no treatment, indicating a low level of Stat3 activity (Fig. 1A). HF-LPLI at both 80 and 120 $J{\cdot}cm^{-2}$ resulted in nuclear translocation of Stat3, suggesting that Stat3 could be activated by HF-LPLI (Fig. 1A). Furthermore, quantitative analysis of Stat3 fluorescence emission intensities in the nucleus showed that Stat3 began to translocate to the nucleus at 20 min, reached a peak at 40 min, and then remained unchanged for up to 3 h after both 80 and 120 $J{\cdot}cm^{-2}$ HF-LPLI (Fig. 1B). However, a higher level of Stat3–YFP nuclear intensity was seen after 120 $J{\cdot}cm^{-2}$ HF-LPLI than after 80 $J{\cdot}cm^{-2}$ HF-LPLI, indicating a higher level of Stat3 activation under 120 $J{\cdot}cm^{-2}$ HF-LPLI. Interleukin-6 (IL-6) was used as a positive control to induce Stat3 nuclear translocation. As shown in Fig. 1A, IL-6 caused a rapid translocation of Stat3 to the nucleus, indicating rapid activation of Stat3. Quantitative data showed that the dynamics of Stat3 in response to IL-6 had a different pattern from that under HF-LPLI (Fig. 1B): the level of Stat3–YFP intensity in the nucleus increased immediately after treatment, reached a peak at $\sim$ 40 min, and then decreased regularly, indicating the activation and recovery process of Stat3 under IL-6 stimulation.

To identify whether Stat3 was activated in time-dependent and dose-dependent manner by HF-LPLI, we used western blotting analysis to detect the phosphorylation levels of Stat3 on the activatory Tyr705 under different time and laser dose treatments. An obvious increase in the phosphorylation level of Stat3 at Tyr705 was detected at 20 min after HF-LPLI. The level reached the highest plateau at 40 min postirradiation, and remained unchanged thereafter (Fig. 1C). The results showed that Stat3 was activated by HF-LPLI in a time-dependent manner. We also determined the phosphorylation levels of Stat3 (Tyr705) under HF-LPLI from 20 to 240 $J{\cdot}cm^{-2}$. We found that the increase in phosphorylated Stat3 (Tyr705) level correlated positively with the laser dose (Fig. 1D),

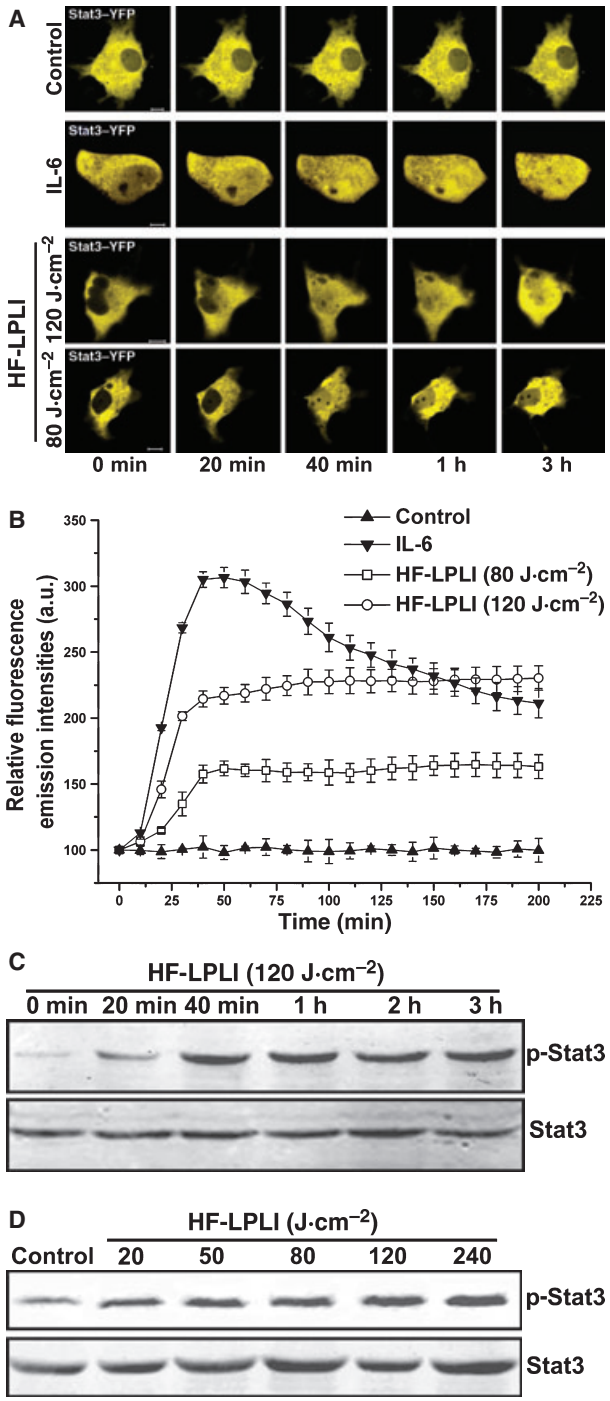

Fig. 1. HF-LPLI induces Stat3 activation in a time-dependent and dose-dependent manner. (A) Representative time-series images of Stat3–YFP after different treatments ($n = 5$). Cells expressing Stat3–YFP were starved for at least 16 h and then treated with HF-LPLI at 80 or 120 J·cm^{-2}. Cells without treatment were used as the control. IL-6 (100 ng·mL^{-1}) was used as a positive control to induce Stat3 nuclear translocation. The fluorescent images were recorded with an LSM510 microscope. Bar: 10 μm. Both 80 and 120 J·cm^{-2} HF-LPLI caused Stat3 nuclear translocation, as indicated by the increase in the Stat3–YFP intensities in the nucleus. (B) Quantitative analysis of relative Stat3–YFP fluorescence emission intensities in the nucleus in cells that received indicated treatments. The data represent mean ± SEM of five independent experiments (10 cells per condition). (C, D) Representative western blotting assay for detection of the levels of endogenous Stat3 phosphorylation (Tyr705) at indicated time points after HF-LPLI (120 J·cm^{-2}) (C) or at different irradiation doses of 20–240 J·cm^{-2} 1 h after irradiation (D) ($n = 3$). The data show that HF-LPLI induces Stat3 activation, as indicated by the increase in phosphorylation levels of Stat3, in a time-dependent and dose-dependent manner.

showing that Stat3 was activated by HF-LPLI in a dose-dependent manner.

Activation of Stat3 inhibits apoptosis induced by HF-LPLI

Obvious cell apoptosis caused by HF-LPLI (120 J·cm^{-2}) was indicated by chromatin condensation and nuclear fragmentation in cells stained with Hoechst 33258 fluorescent dyes (Fig. 2A). Furthermore, to evaluate the potential biological effect of Stat3 activation on Bax activation (which is directly related to the mitochondrial translocation of Bax) under HF-LPLI (120 J·cm^{-2}), cells were transfected with cyan fluorescent protein (CFP)–Bax or cotransfected with pCFP–Bax and dominant negative (DN) Stat3(Y705F)–YFP plasmid. Bax was uniformly distributed in cells with no treatment (Fig. 2B). Staurosporine (STS) was used as a positive control to induce Bax activation (Fig. 2B,C). Bax was activated by HF-LPLI at 263 min post-treatment (Fig. 2B,C). Overexpression of Stat3(Y705F)–YFP significantly promoted Bax activation for 65 min, revealing an inhibitory effect of Stat3 on Bax activation during the apoptotic process induced by HF-LPLI.

To determine statistically whether Stat3 activation could inhibit HF-LPLI-induced apoptosis, cell apoptosis was analyzed by flow cytometry based on annexin V–fluorescein isothiocyanate (FITC)/propidium iodide (PI) double staining. The results showed that 80 J·cm^{-2} HF-LPLI induced 17.3% cell apoptosis 6 h post-treatment, whereas 120 J·cm^{-2} HF-LPLI induced 21.4% cell apoptosis (Fig. 2D). We also found that Stat3(Y705F) overexpression enhanced cellular apoptosis, whereas overexpression of Stat3C (a constitutively active form of Stat3) reduced cellular apoptosis under HF-LPLI at both doses (Fig. 2D,E). These results show that Stat3 activation inhibited the apoptosis induced by HF-LPLI.

To further determine whether Stat3 activation could inhibit HF-LPLI-induced apoptosis, cell apoptosis was

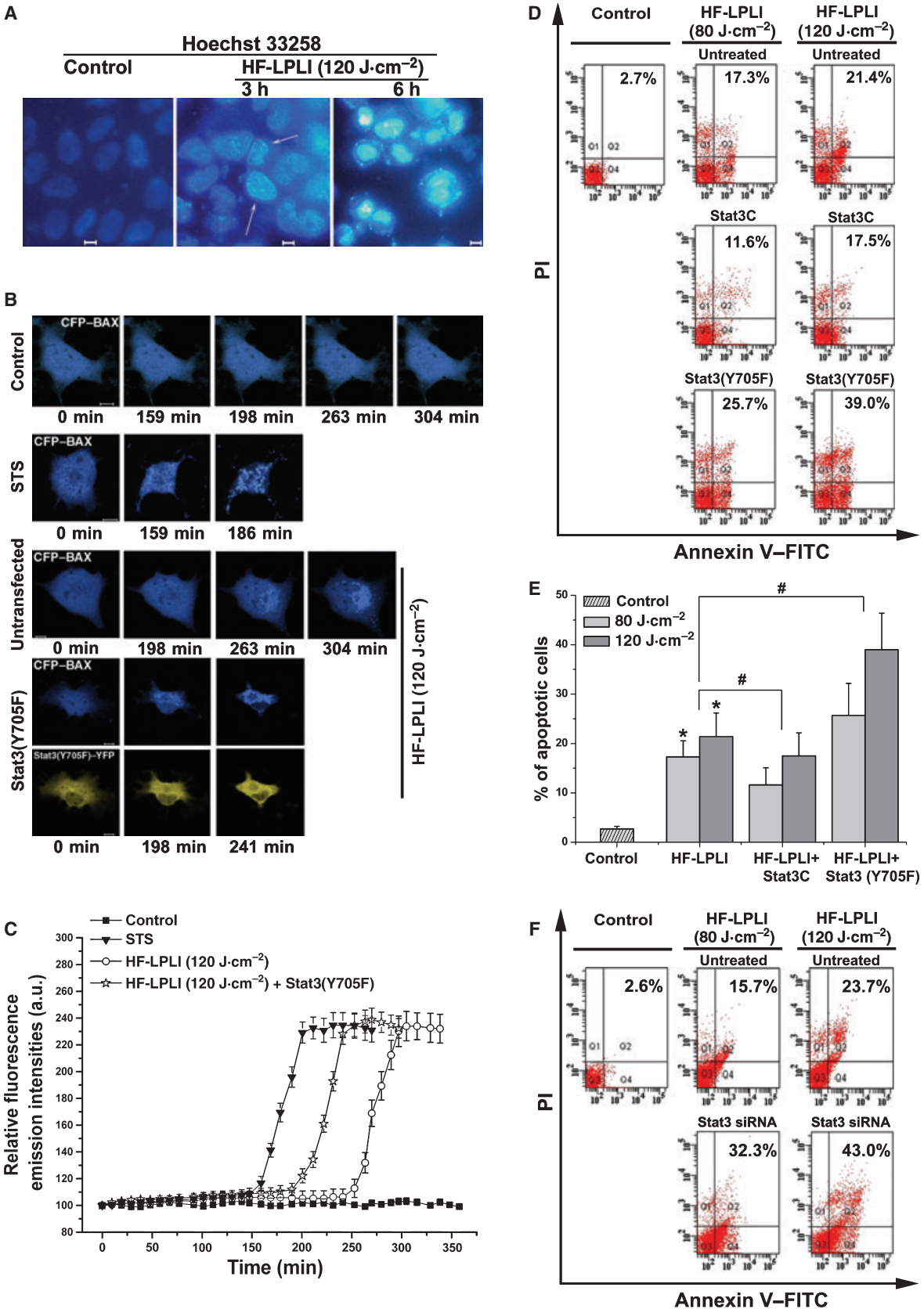
A
Hoechst 33258
Control
HF-LPLI (120 J·cm−2)
3 h
6 h
B
CFP–BAX
Control
0 min
159 min
198 min
263 min
304 min
STS
0 min
159 min
186 min
Untransfected
0 min
198 min
263 min
304 min
Stat3(Y705F)
Stat3(Y705F)–YFP
0 min
198 min
241 min
HF-LPLI (120 J·cm−2)
C
Control
STS
HF-LPLI (120 J·cm−2)
HF-LPLI (120 J·cm−2) + Stat3(Y705F)
Relative fluorescence emission intensities (a.u.)
Time (min)
D
Control
HF-LPLI (80 J·cm−2)
HF-LPLI (120 J·cm−2)
Untreated
2.7%
17.3%
21.4%
Stat3C
11.6%
17.5%
Stat3(Y705F)
25.7%
39.0%
PI
Annexin V–FITC
E
Control
80 J·cm−2
120 J·cm−2
% of apoptotic cells
Control
HF-LPLI
HF-LPLI+ Stat3C
HF-LPLI+ Stat3 (Y705F)
F
Control
HF-LPLI (80 J·cm−2)
HF-LPLI (120 J·cm−2)
Untreated
2.6%
15.7%
23.7%
Stat3 siRNA
32.3%
43.0%
PI
Annexin V–FITC

Fig. 2. The protective effect of Stat3 on HF-LPLI-induced cell apoptosis. (A) Hoechst 33258 nuclear staining revealed morphological changes of cells treated with HF-LPLI at 120 J·cm^{-2}. Bar: 10 μm. The data show that HF-LPLI causes cell apoptosis, as indicated by nuclear condensation and chromatin fragmentation ($n = 3$). (B) Representative time-series images of cells expressing CFP–Bax under HF-LPLI with or without DN Stat3(Y705F)–YFP overexpression. Bar: 10 μm. Cells treated with STS (1 μM) were used as a positive control. The data show that Stat3 inhibits Bax activation induced by HF-LPLI ($n = 5$). (C) Quantitative analysis of relative CFP–Bax fluorescence emission intensities in the punctated dots in cells that received the indicated treatments. The data represent mean ± SEM of five independent experiments (10 cells per condition). (D) Representative flow cytometry analysis for the levels of cell apoptosis 6 h after irradiation in response to the indicated treatments, based on annexin V/PI double staining. The data show that Stat3 protects cells from HF-LPLI-induced apoptosis ($n = 3$). (E) Graphical quantitation of the apoptosis rates. The data represent mean ± SEM of three independent experiments (*$P < 0.05$ versus control cells, #$P < 0.05$ versus indicated cells, Student's *t*-test.) (F) Flow cytometry analysis for the levels of cell apoptosis 6 h after irradiation in response to the indicated treatments, based on annexin V/PI double staining. The data further indicate that Stat3 protects cells from HF-LPLI-induced apoptosis.

analyzed by flow cytometry after transfection with Stat3 small interfering RNA (siRNA). The results showed that Stat3 siRNA expression greatly enhanced cellular apoptosis under both 80 and 120 J·cm^{-2} HF-LPLI (Fig. 2F). This suggested that Stat3 activation inhibited the apoptosis induced by HF-LPLI.

Src plays a major role in Stat3 activation induced by HF-LPLI

To determine whether Src was involved in Stat3 activation induced by HF-LPLI, we pretreated cells with 4-amino-5-(4-methylphenyl)-7-(t-butyl) pyrazolo(3,4-d)-pyrimidine (PP1), a selective inhibitor of Src family kinases, and observed the changes in the subcellular localation of Stat3. Cells with no treatment were used as the control (Fig. 3A). As shown in Fig. 3A, HF-LPLI with PP1 pretreatment resulted in reduced nuclear translocation of Stat3 in comparison with HF-LPLI alone, suggesting that Src participated in Stat3 activation under HF-LPLI. PP1 pretreatment alone had no effect on the subcellular location of Stat3 (Fig. 3A). Quantitative analysis of Stat3 fluorescence emission intensities in the nucleus showed that PP1 pretreatment largely inhibited the nuclear translocation of Stat3 upon HF-LPLI, suggesting that Src played a major role in Stat3 activation (Fig. 3B).

Western blotting analysis was used to detect the phosphorylation levels of Stat3 (Tyr705) when cells were treated with 120 J·cm^{-2} HF-LPLI in the presence of PP1. We found that PP1 pretreatment greatly inhibited the increase in phosphorylation levels of Stat3 induced by HF-LPLI (Fig. 3C), showing that Src was the dominant upstream kinase of Stat3.

To confirm that Src was the dominant kinase in Stat3 activation, we separately treated cells with SU6656, a selective Src family kinase inhibitor, and AG490, a JAK-specific inhibitor. We then observed the phosphorylation levels of Stat3 (Tyr705) after HF-LPLI. The results showed that HF-LPLI with SU6656 pretreatment resulted in reduced phosphorylation of Stat3 in comparison with HF-LPLI alone (Fig. 3D), indicating that Src was involved in Stat3 activation. HF-LPLI with AG490 pretreatment also resulted in reduced phosphorylation of Stat3, but the inhibitory effect was much lower than that induced by HF-LPLI with SU6656 pretreatment (Fig. 3E), indicating a minor role of JAKs in Stat3 activation. The two results suggested that Src was the dominant upstream kinase of Stat3 under HF-LPLI.

To further confirm the above result, we separately pretreated cells with SU6656 and AG490, and observed cellular apoptosis under HF-LPLI (120 J·cm^{-2}). This result showed that HF-LPLI induced 24.3% cellular apoptosis 6 h post-treatment. Both SU6656 and AG490 pretreatment enhanced apoptosis after HF-LPLI, but the levels of apoptosis enhanced by SU6656 pretreatment were larger than those induced by AG490 pretreatment (Fig. 3F). This result indicated that Src played a major role in Stat3 activation and that activation of the Src–Stat3 pathway could inhibit the apoptosis induced by HF-LPLI.

Src is activated by HF-LPLI

To identify the involvement of Src in HF-LPLI-induced apoptosis, we transfected cells with a Src reporter plasmid that could be used to image and quantify the spatiotemporal activation of Src in living cells [16,18]. As shown in Fig. 4A, the YFP/CFP emission ratio quickly decreased after either 80 or 120 J·cm^{-2} HF-LPLI, indicating the rapid activation of Src. From quantitative analysis of the YFP/CFP emission ratio of the Src reporter, we found that the decrease in the YFP/CFP emission ratio peaked at $\sim$ 5 min post-treatment, and remained relatively invariant thereafter (Fig. 4B). In addition, 120 J·cm^{-2} HF-LPLI induced a more sharp decrease in the YFP/CFP emission ratio than 80 J·cm^{-2} HF-LPLI, showing that the level of Src activation was positively correlated with the dose of HF-LPLI. Cells with no treatment were used as the control (Fig. 4A). Epidermal

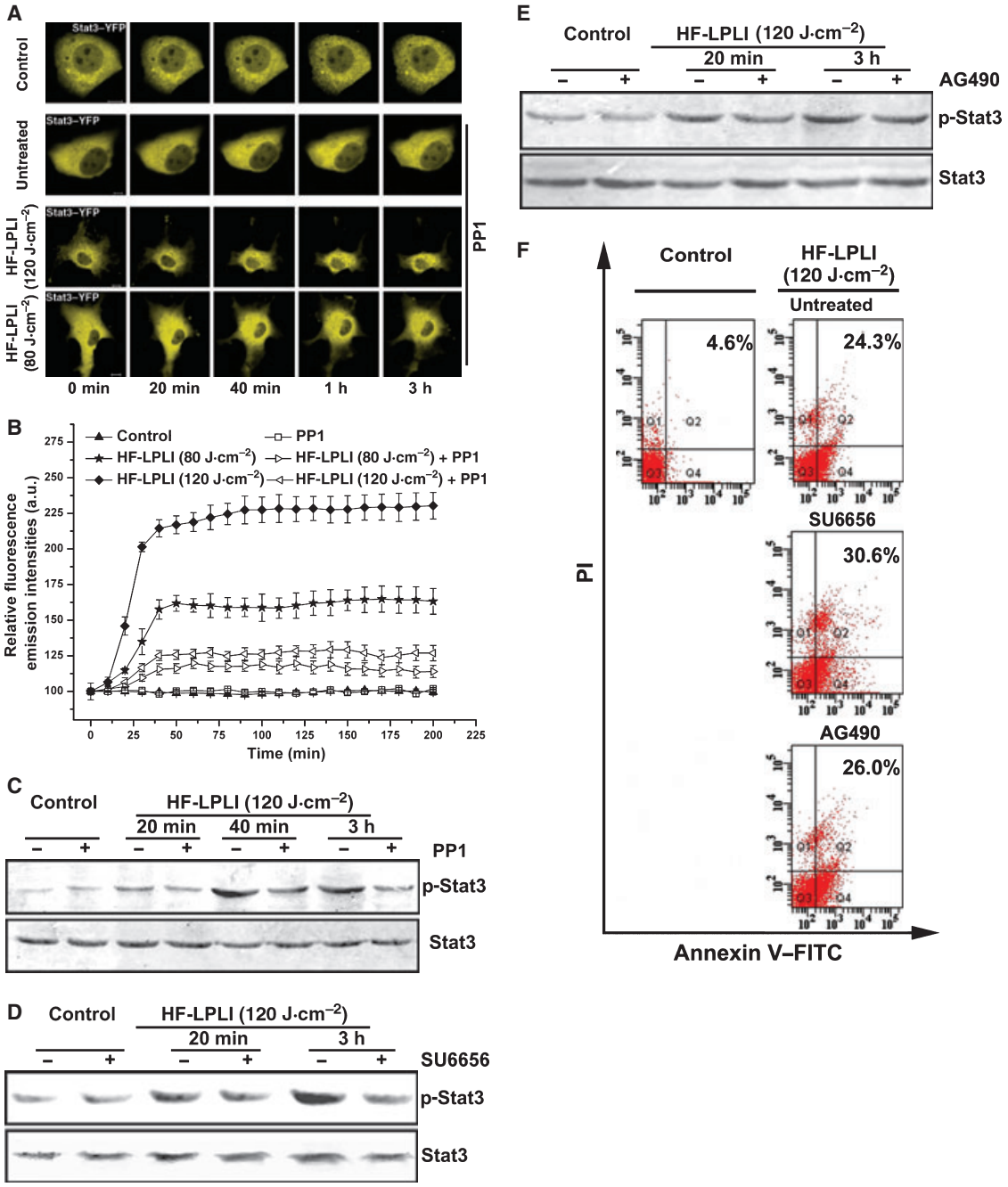

Fig. 3. Src is involved in Stat3 activation under HF-LPLI. (A) Representative time-series images of Stat3–YFP in cells after different treatments (n = 5). Cells expressing Stat3–YFP were starved for at least 16 h and then treated with 80 or 120 J·cm^{-2} HF-LPLI in the presence of PP1 (10 μM). The fluorescent images were recorded with an LSM510 microscope. Bar: 10 μm. Src was involved in Stat3 nuclear translocation, because the nuclear accumulation of Stat3–YFP was much lower in HF-LPLI-treated cells in the presence of PP1 than in cells treated with HF-LPLI alone (Fig. 1A). (B) Quantitative analysis of relative Stat3–YFP fluorescence emission intensities in the nucleus in cells that received the indicated treatments. The data represent mean ± SEM of five independent experiments (10 cells per condition). (C, D) Representative western blotting assays for detection of the levels of endogenous Stat3 phosphorylation (Tyr705) at the indicated time points under different treatments (n = 3). The data show that Src is essential for Stat3 activation, as indicated by the significant decrease in Stat3 phosphorylation levels in the presence of PP1 (10 μM) (C) or SU6656 (50 nM) (D) and the weak decrease in Stat3 phosphorylation levels in the presence of AG490 (50 μM) (E) under 120 J·cm^{-2} HF-LPLI. (F) Flow cytometry analysis for the levels of cell apoptosis 6 h after irradiation in response to the indicated treatments, based on annexin V/PI double staining. The data show that Src was the dominant upstream kinase of Stat3 under HF-LPLI, and that Stat3 activation protects cells from HF-LPLI-induced apoptosis.

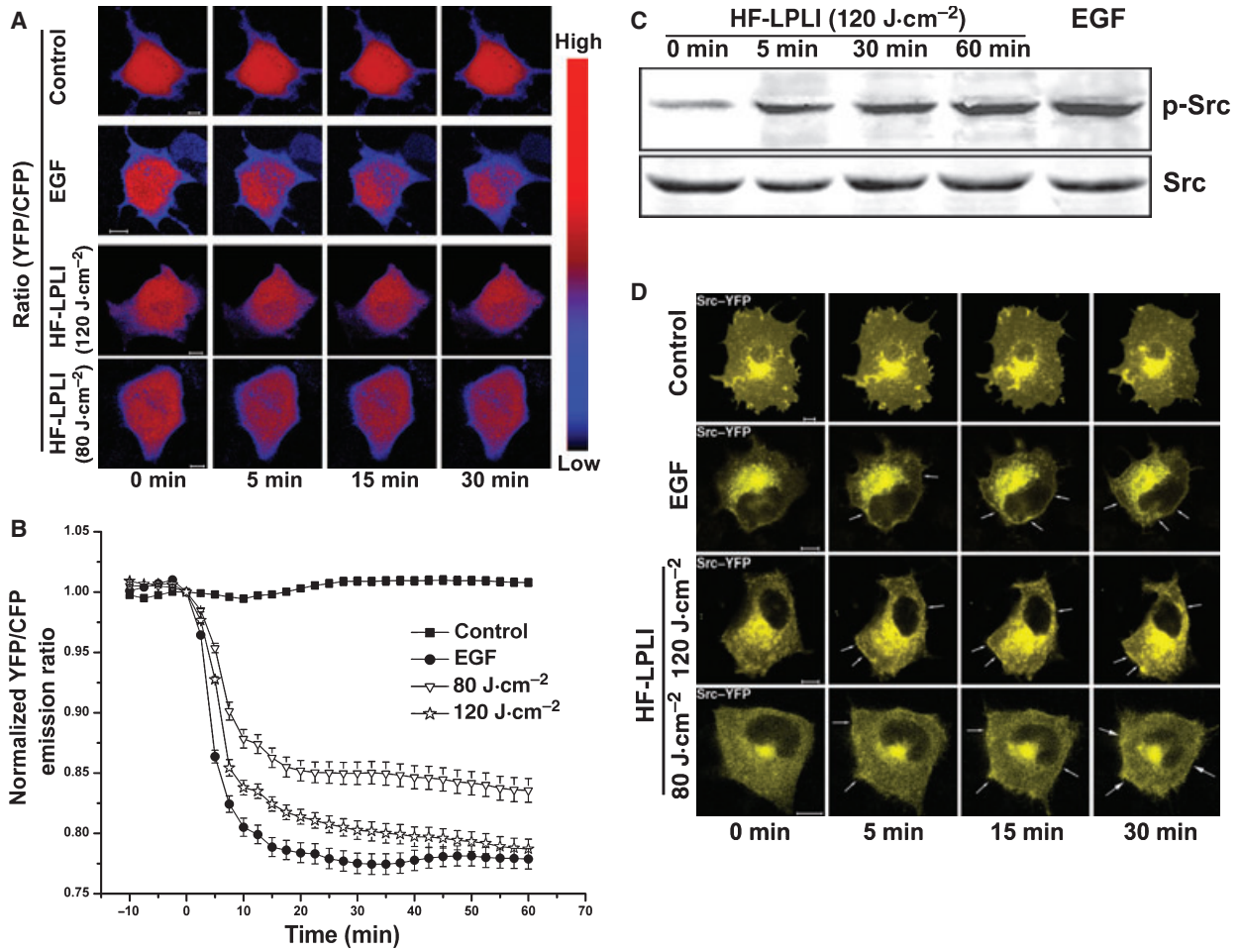

Fig. 4. The activation of Src induced by HF-LPLI. (A) Representative pseudocolor image series of the YFP/CFP emission ratio at the indicated time points upon stimulation with HF-LPLI (n = 5). Cells expressing Src reporter were starved for at least 16 h, and then treated with HF-LPLI at 80 or 120 J·cm^{-2}. EGF (50 ng·mL^{-1}) was used as a positive control to induce Src activation. The fluorescent images were recorded with an LSM510 microscope. Bar: 10 μm. Both 80 and 120 J·cm^{-2} HF-LPLI caused Src activation, as indicated by the decrease in the YFP/CFP emission ratio. (B) Quantitative analysis of the YFP/CFP emission ratio in cells that received the indicated treatments. The data represent mean ± SEM of five independent experiments (10 cells per condition). (C) Representative western blotting assay for detection of the levels of Src phosphorylation (Tyr416) at the indicated time points after 120 J·cm^{-2} HF-LPLI (n = 3). The data show that HF-LPLI induces Src activation, as indicated by the increase in the phosphorylation levels of Src. (D) Representative time-series images of Src–YFP membrane translocation after HF-LPLI (n = 5). Cells expressing Src–YFP were starved for at least 16 h, and then treated with 80 or 120 J·cm^{-2} HF-LPLI. Bar: 10 μm. Both 80 and 120 J·cm^{-2} HF-LPLI caused Src activation, as indicated by the Src–YFP membrane translocation.

growth factor (EGF) was used as a positive control to induce Src activation, which was shown by a rapid and robust decrease in the YFP/CFP emission ratio (Fig. 4A,B).

Western blotting analysis was used to detect the phosphorylation levels of Src on the activatory Tyr416 under HF-LPLI. An obvious increase in phosphorylated Src (Tyr416) levels was detected at 5 min after 120 J·cm^{-2} HF-LPLI, and the levels remained relatively constant thereafter (Fig. 4C), indicating the activation of Src. EGF was used as positive control to induce the increase in phosphorylated Src (Tyr416) levels.

To further confirm Src activation by HF-LPLI, we observed the membrane translocation of Src, which was accompanied by Src activation [19]. Cells were transfected with Src–YFP, and after 48 h of expression, positive transfected cells were treated with HF-LPLI at 80 or 120 J·cm^{-2}. We found that Src was mainly present in the perinuclear area and partly located at the cell membrane with no treatment (Fig. 4D), indicating a low level of Src activity. HF-LPLI at either 80 or 120 J·cm^{-2}

resulted in the membrane translocation of Src at 5 min post-treatment, and the membrane translocation remained relatively steady thereafter, suggesting that Src was activated by HF-LPLI (Fig. 4D). EGF was used as a positive control to induce Src membrane translocation (Fig. 4D).

ROS are essential for the activation of Stat3 and Src induced by HF-LPLI

To detect the generation of ROS after HF-LPLI treatment, cells were monitored by measuring changes in fluorescence resulting from the oxidation of intracellular H_2DCFDA (nonfluorescent) to DCF (fluorescent), and the intensity of DCF fluorescence indicates the relative amount of ROS production. Cells were incubated with 10 μmol H_2DCFDA for 30 min in an incubator. The typical time-course images of cells loaded with H_2DCFDA after laser irradiation are shown in Fig. 5A. HF-LPLI at both 80 and 120 J·cm^{-2} resulted in a gradual increase of DCF fluorescence intensity, indicating the generation of ROS. The DCF fluorescence intensity reached a plateau $\sim$ 60 min after laser irradiation of 120 J·cm^{-2} (Fig. 5A,B) and after $\sim$ 80 min after laser irradiation of 80 J·cm^{-2} (Fig. 5A,B). Cells with no treatment were used as the control (Fig. 5A).

To confirm whether ROS are indispensable for Src and Stat3 activation, we used the ROS scavenger vitamin C to eliminate ROS generated by HF-LPLI, and then detected the activity of Stat3. As shown in Fig. 5C, the nuclear translocation of Stat3 induced by either 80 or 120 J·cm^{-2} HF-LPLI was totally blocked by vitamin C pretreatment, indicating the critical role of ROS in Stat3 activation. The quantitative analysis of Stat3 fluorescence intensities gave a similar result (Fig. 5D).

To further identify the essential role of ROS in Stat3 activation, we used western blotting analysis to detect the phosphorylation levels of Stat3 (Tyr705) under 120 J·cm^{-2} HF-LPLI in the presence of vitamin C or *N*-acetylcysteine (NAC). The results showed that the increase in the phosphorylation levels of Stat3 (Tyr705) induced by HF-LPLI was completely abolished when cells were preincubated with vitamin C (Fig. 5E) or NAC (Fig. 5F), suggesting that ROS were essential for Stat3 activation.

To verify the critical role of ROS in Src activation under 120 J·cm^{-2} HF-LPLI, we detected the phosphorylation levels of Src (Tyr416) after HF-LPLI in the presence of vitamin C. We found that the increase in phosphorylation levels of Src (Tyr416) was completely inhibited by vitamin C pretreatment (Fig. 5G), indicating the critical role of ROS for Src activation.

Discussion

In the present study, we proved for the first time that Stat3 is involved in HF-LPLI-induced apoptosis in COS-7 cells. The salient findings of the present study can be summarized as follows: (a) HF-LPLI activated Stat3 in a time-dependent and dose-dependent manner; (b) Stat3 activation inhibited HF-LPLI-induced apoptosis by inhibiting Bax activation; (c) Src was the major upstream kinase of Stat3 activation under HF-LPLI; and (d) ROS generation induced by HF-LPLI was essential for activation of the Src–Stat3 signaling pathway. In conclusion, these findings demonstrated that the ROS–Src–Stat3 pathway mediated negative feedback inhibition of apoptosis under HF-LPLI.

It is rational to speculate that the antiapoptosis target proteins of Stat3 execute the inhibition of apoptosis under HF-LPLI, as activated Stat3 molecules can dimerize and accumulate in the nucleus, where they induce transcription of many target genes, such as those encoding Bcl-2, Bcl-xL, Mcl-1, survivin, cyclin D1 and c-Myc [20–22]. Bcl-2, Bcl-xL and Mcl-1 are important antiapoptotic Bcl-2 family proteins, and have been reported to inhibit Bax activation under various apoptotic treatments [23]. In addition, Bax activation is an important step during HF-LPLI-induced apoptosis [6]. Therefore, we believed that one of the crosslinks between antiapoptotic pathways and proapoptotic pathways under HF-LPLI was Stat3, through transcriptional upregulation of the Bcl-2 antiapoptotic proteins to attenuate Bax activation. Our results supported this view, because inhibition of Stat3 by DN Stat3(Y705F) overexpression obviously promoted Bax activation (Fig. 2B). On the other hand, the expression of survivin, an inhibitor of apoptosis, has also been found to be regulated by constitutively activated Stat3 in cancer cells [24,25], and thus survivin may also participate in the negative feedback inhibition of apoptosis induced by HF-LPLI. Also, cyclin D1 and c-Myc have been reported to potentially control the growth and survival of cells [26], so these two proteins may also be involved in the Stat3-mediated inhibition of apoptosis.

Why are Stat3–YFP fluorescence emission intensities in the nucleus different at the zero time point? The activity of Stat3 is low in COS-7 cells without any treatment (Fig. 1A,C). However, the amount of Stat3 protein in the nucleus is different in separate cells, and the possible reason may be that the microenvironments of separate cells are different; for example, there are different concentrations of growth factors and cytokines. These factors could influence the activity of Stat3, and thus influence the amount of Stat3 protein in the nucleus.

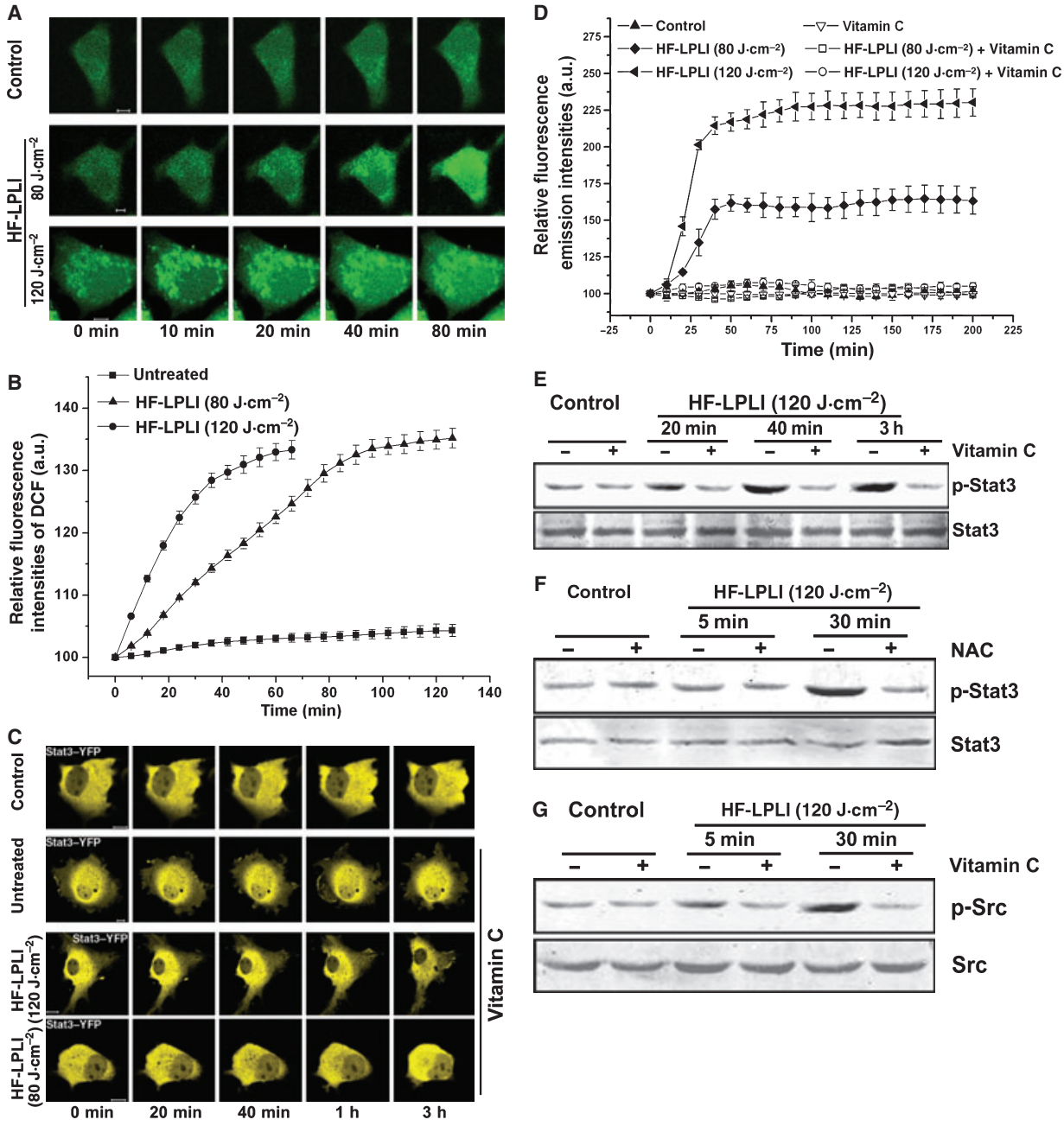

Fig. 5. HF-LPLI-induced activation of Stat3 and Src are both redox sensitive. (A) Representative time-series images of DCF staining after HF-LPLI stimulation (n = 5). Cells were prestained with DCF, and then treated with 80 or 120 J·cm^{-2} HF-LPLI. The fluorescent images were recorded with an LSM510 microscope. Bar: 10 μm. The data show the generation of ROS after HF-LPLI at both 80 and 120 J·cm^{-2}. (B) Quantitative analysis of relative DCF fluorescence intensities in cells that received the indicated treatments. The data represent mean ± SEM of five independent experiments (10 cells per conditions). (C) Representative time-series images after HF-LPLI stimulation in the presence of vitamin C (100 μM) (n = 5). Cells expressing Stat3–YFP were starved for at least 16 h, and then treated with 80 or 120 J·cm^{-2} HF-LPLI in the presence or absence of vitamin C. The fluorescent images were recorded with an LSM510 microscope. Bar: 10 μm. The data show that Stat3 activation is redox sensitive, as indicated by the abolition of the increase of Stat3–YFP intensities in the nuclei of cells preincubated with vitamin C induced by 80 or 120 J·cm^{-2} HF-LPLI. (D) Quantitative analysis of relative Stat3–YFP fluorescence emission intensities in nuclei of cells that received the indicated treatments. The data represent mean ± SEM of five independent experiments (10 cells per condition). (E–G) Representative western blotting assay for detection of the levels of Stat3 phosphorylation (Tyr705) and Src phosphorylation (Tyr416) at the indicated time points after different treatments (n = 3). The data suggest that ROS are essential for the activation of Stat3 and Src.

What is the mechanism of ROS generation under HF-LPLI? It has been widely reported that light is absorbed by endogenous photosensitizers (porphyrins or cytochromes) that are predominantly located in the plasma membrane, mitochondria or lysomes after HF-LPLI, and the activation of photosensitizers results in ROS production [27]. ROS, as common secondary messengers, play important roles in photosignal transduction. Vitamin C, as an important antioxidant that protects organisms from oxidative stress, could scavenge the ROS generated by HF-LPLI [6]. Our data showed that vitamin C pretreatment totally blocked the activation of Stat3 and Src (Fig. 5), indicating the essential role of ROS in Stat3 and Src activation. This finding provides evidence regarding the important role of ROS as secondary messengers in the stimulatory effect of HF-LPLI.

What are the possible pathways of Src activation by ROS generated by HF-LPLI? The activation of Src by ROS can be partially explained by the ability of ROS to oxidize thiol groups in Src or to inactivate protein tyrosine phosphatases (PTPs). ROS can directly oxidize specific cysteines in Src, resulting in a conformational change that is necessary for Src activation. Redox regulation is considered to be a key feature of Src function [28]. Besides direct oxidation, ROS are widely accepted as inactivating PTPs [29], thereby shifting the equilibrium in favor of kinase activation [30,31]. Transient inactivation of PTPs by ROS generated by B-lymphocyte antigen receptor activation is considered to be sufficient to activate the Src family kinase Lyn [32].

Is Stat3 activation a general event in response to different apoptotic stimuli besides HF-LPLI? We used STS (1 μM) to induce apoptosis, and showed that Stat3 was not activated in the apoptosis of COS-7 cells (data not shown). STS is a traditional apoptosis-inducing agent. STS stimulation engages a cell death pathway involving ROS production and mitochondrial dysfunction in PC12 cells [33]. Otherwise, STS at a relatively low concentration (50 nM) is widely used as a broad serine/threonine kinase inhibitor, and has been shown to have no significant effect on the activation of Stat3 [34]. However, the reason why Stat3 is activated by HF-LPLI but not by STS has not been confirmed. The differences in the apoptotic processes induced by HF-LPLI and STS could provide a theoretical basis for their use.

The mechanism of apoptosis induced by HF-LPLI is not well understood. Knowledge of such a mechanism is necessary for the clinical application of low-power laser therapies. It can provide a new stimulator to trigger cell apoptosis, as it is well known that apoptosis plays an important role in physiological and pathological conditions [35,36].

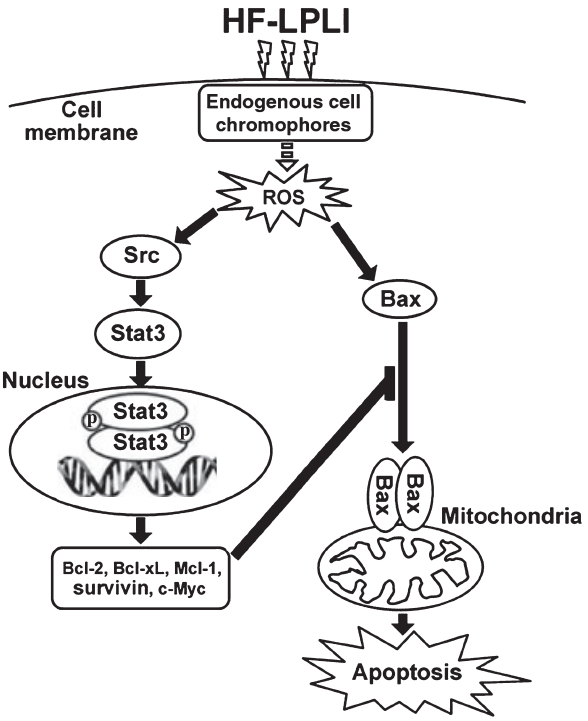

Fig. 6. Model of the negative feedback inhibition induced by Stat3 activation on stimulation with HF-LPLI. ROS are generated through activation of endogenous cell chromophores by HF-LPLI, and ROS generation induces Bax oligomerization and cell apoptosis. At the same time, the ROS–Src–Stat3 pathway is activated, and the antiapoptosis target proteins are expressed. These proteins are responsible for the inhibition of Bax activation, and thus inhibit apoptosis.

In conclusion, we have shown the activation of the ROS–Src–Stat3 signaling pathway in COS-7 cells stimulated with HF-LPLI, and that activation of this pathway mediates negative feedback inhibition of HF-LPLI-induced apoptosis (Fig. 6). Intracellular negative feedback mechanisms can act in a cell-autonomous manner in downregulating pathway activity during evolution. These mechanisms provide effective ways of modulating the cellular response to an instructive signal within cells, and have been widely used to regulate the activity of signaling pathways [37]. The discovery of the unique signaling pathway in our research will enhance our current understanding of negative feedback mechanisms.

Experimental procedures

Chemicals and antibodies

Lipofectamine 2000 Reagent was purchased from Invitrogen (Carlsbad, CA, USA). Recombinant human IL-6 was purchased from Peprotech (Rocky Hill, NJ, USA). EGF (diluted in dimethylsulfoxide) was purchased from PeproTech (Rocky Hill). Vitamin C was purchased from Sigma

(St Louis, MO, USA). PP1 was purchased from Invitrogen (Carlsbad, CA, USA). H_2DCFDA was purchased from Dojindo Laboratories (Kumamoto, Japan). SU6656 and AG490 were purchased from CalBiochem (La Jolla, CA, USA). Antibodies against Stat3 and phosphorylated Stat3 (Tyr705) were purchased from Cell Signaling Technology (Danvers, MA, USA). Antibody against Src was purchased from Cell Signaling Technology (Beverly, MA, USA). Antibody against phosphorylated Src (Tyr416) was purchased from Upstate Biotechnology (New York, NY, USA).

Construction of siRNA expression vectors of Stat3

An siRNA target located in the SH2 domain of Stat3 (nucleotides 2144–2162; Genbank accession no. NM00315) was chosen for use [38]. The sequence of Stat3-specific hairpin RNA is as follows: GCAGCAGCTGAACAACATGT TCAAGAGACATGTTGTTCAGCTGCTGCTTTTT. This oligonucleotide contains a sense strand of 20 nucleotides followed by a short spacer (loop sequence: TTCAAGA GA), the antisense strand, and five Ts (terminator).

Cell culture and transfection

COS-7 cells were cultured in DMEM (Life Technologies, Grand Island, NY, USA) supplemented with 15% fetal bovine serum (Gibco, Grand Island, NY, USA), 50 $U{\cdot}mL^{-1}$ penicillin, and 50 $mg{\cdot}mL^{-1}$ streptomycin. Cells were grown at 37 °C in a water-saturated atmosphere at 5% CO_2. Transfection of all plasmids and Stat3 siRNA was carried out with Lipofectamine 2000, according to the manufacturer's instructions.

HF-LPLI

For irradiation of cells in confocal experiments, a 633 nm He–Ne laser inside a confocal laser scanning microscope (LSM510-ConfoCor2; Zeiss, Jena, Germany) was used. Laser irradiation was performed through the objective lens (× 40/NA1.3) of the inverted microscope in laser scanning mode. In this setup, only the cells under observation were irradiated by the laser. The output laser power through the objective lens was measured with a power meter. The cells in the selected area were irradiated for 10 min with fluences of 80 or 120 $J{\cdot}cm^{-2}$. For irradiation of cells in other experiments, an He–Ne laser (HN-1000; Guangzhou, China; 633 nm) was used to irradiate cells for 10 min with fluences of 20, 50, 80, 120 and 240 $J{\cdot}cm^{-2}$, respectively.

Imaging analysis of living cells

For imaging of single cells, the confocal laser scanning microscope system (LSM510-ConfoCor2) was used. The system was equipped with an Ar ion laser (30 mW) and an He–Ne laser (5 mW) for excitation illumination. To avoid fluorescence saturation and bleaching, the illumination power was reduced from 3% to 0.3% of the maximum power of the excitation lasers. All images were recorded with a Plan-Neofluar × 40/NA1.3, oil-immersed objective lens before and after laser irradiation. Cells were also maintained at 37 °C and 5% CO_2 during imaging with the mini-type culture chamber. The imaging process was as follows. Stat3–YFP, DN Stat3(Y705F)–YFP and Src–YFP were excited with the Ar ion laser: 514 nm excitation wavelength, 458/514 nm main dichroic beam splitter, and 530 nm long-pass emission detection filter. CFP–Bax was excited with the Ar ion laser: 458 nm excitation wavelength, 458 nm main dichroic beam splitter, and 470–500 nm bandpass emission detection filter.

Fluorescence resonance energy transfer (FRET) analysis of Src reporter

COS-7 cells transfected with Src reporter were grown in DMEM for 36 h, and FRET analysis was performed on a commercial Laser Scanning Microscope (LSM510/ConfoCor2) combination system (Zeiss). The Src reporter is composed of CFP, the SH2 domain, a flexible linker, the Src substrate peptide and YFP. Before Src phosphorylation, the juxtaposition of CFP and YFP yields a high FRET. On Src phosphorylation, the substrate peptide can bind to the phosphopeptide-binding pocket of the SH2 domain and separate YFP from CFP, thus decreasing the FRET [16,18].

For excitation, the 458 nm line of an Ar ion laser was attenuated with an acousto-optical tunable filter, reflected by a dichroic mirror (main beam splitter HFT458), and focused through a Zeiss C-Apochromat × 40/NA1.3 objective onto the sample. The emission fluorescence was split by a second dichroic mirror (secondary beam splitter NFT515) into two separate channels: the 470–500 nm bandpass (CFP channel) and the 530 nm long pass (YFP channel). For intracellular measurements, the desired measurement position was chosen in the laser scanning microscope image. After the whole area of observed cells had been chosen, the average fluorescence intensities of CFP and YFP channels and the background were obtained. The background-subtracted fluorescence intensity of YFP divided by the background-subtracted fluorescence intensity of CFP is the YFP/CFP ratio. For each experiment, the YFP/CFP ratio over time was normalized to 1 at the zero time point. The cell images were presented in pseudocolor to highlight the changes in the YFP/CFP fluorescence intensity ratio over time.

Morphological examination of apoptotic cells

As a direct confirmation, cell apoptosis was morphologically evaluated by nuclear staining with Hoechst 33258 dye.

Cells (1×10^6) were treated with HF-LPLI (120 J·cm^{-2}) and incubated for 3 and 6 h in 35 mm dishes. Hoechst 33258 (10 μg·mL^{-1}) was added to the dishes, and the cells were incubated at 37 °C for 30 min in the dark. Fluorescence images of the normal and apoptotic cells were examined with a modified commercial microscope system equipped with a mercury lamp (bandpass filter: 365 ± 6 nm), a 395 nm dichroic mirror and a longpass 397 nm emission filter (LSM510/ConfoCor2; Zeiss). The fluorescence images were collected via a Zeiss C-Apochromat objective (× 40/NA1.3).

Western blotting assay

For western blotting assays, cells were plated in 6 cm Petri dishes. Briefly, cells were washed three times with precooled NaCl/P_i before being scraped. The treated or untreated cells were lysed in a buffer containing 50 mM Tris/HCl (pH 8.0), 150 mM NaCl, 1% Triton X-100, 1 mM Na_3VO_4, 100 mM phenylmethanesulfonyl fluoride and protease inhibitor cocktail set I (Calbiochem). The samples were separated by 10% SDS/PAGE and transferred onto a poly(vinylidene difluoride) membrane (Millipore, Eschborn, Germany). The resulting membrane was blocked with 5% skimmed milk, and incubated with a designated primary antibody and the secondary antibody. The signals were detected with an ODYSSEY Infrared Imaging System (LI-COR; Lincoln, NE, USA). The following antibodies were used for immunoblotting: antibody against phosphorylated Stat3 (Tyr705), antibody against phosphorylated Src (Tyr416), IRDye 700 CW anti-(rabbit IgG), and Alexa - Fluor 800 goat anti-(mouse IgG).

Quantitative analysis of cell apoptosis

For flow cytometry analysis, annexin V–FITC conjugate, PI dyes and binding buffer were used as standard reagents. The analysis was performed on a FACScanto II flow cytometer (Becton Dickinson, Mountain View, CA, USA) with excitation at 488 nm. Fluorescence emission of FITC was measured at 515–545 nm, and fluorescence emission of DNA–PI complexes was measured at 564–606 nm. Cell debris was excluded from analysis by an appropriate forward light scatter threshold setting. Compensation was used wherever necessary.

Statistics

All assays were performed at least three times. All error bars represent standard error of the mean (SEM) ($n \geq 3$). For statistical evaluation, Student's paired *t*-test was used, and significance was defined as $P < 0.05$. For fluorescence emission intensity analysis, a background subtraction was performed for all of the data.

Acknowledgements

This research was supported by the National Basic Research Program of China (2010CB732602), the Program for Changjiang Scholars and Innovative Research Team in University (IRT0829), and the National Natural Science Foundation of China (30870676; 30870658). We thank G. Müller-Newen (Universitätsklinikum RWTH, Aachen, Germany) for kindly providing the Stat3–YFP and DN Stat3(Y705F)–YFP mutant plasmids, U. Walter (University of Wurzburg, Germany) for kindly providing the Src–YFP plasmid, J. Bromberg (Memorial Sloan-Kettering Cancer Center, USA) for kindly providing Stat3C and DN Stat3(Y705F) mutant plasmids, S. Chien (University of California, CA, USA) for kindly providing the plasmid DNA of Src reporters, and C. Andrew (School of Biological Science, University of Manchester, UK) for kindly providing the CFP–Bax plasmid.

References

1 O'Kane S, Shields TD, Gilmore WS & Allen JM (1994) Low intensity laser irradiation inhibits tritiated thymidine incorporation in the hemopoietic cell lines HL-60 and U937. *Lasers Surg Med* **14**, 34–39.
2 Gross AJ & Jelkmann W (1990) Helium–neon laser irradiation inhibits the growth of kidney epithelial cells in culture. *Lasers Surg Med* **10**, 40–44.
3 Ocaña-Quero JM, Perez de la Lastra J, Gomez-Villamandos R & Moreno-Millán M (1998) Biological effect of helium–neon (He–Ne) laser irradiation on mouse myeloma (Sp2-Ag14) cell line in vitro. *Lasers Med Sci* **13**, 214–218.
4 Wang F, Chen TS, Xing D, Wang JJ & Wu YX (2005) Measuring dynamics of caspase-3 activity in living cells using FRET technique during apoptosis induced by high fluence low-power laser irradiation. *Lasers Surg Med* **36**, 2–7.
5 Wu S, Xing D, Wang F, Chen T & Chen WR (2007) Mechanistic study of apoptosis induced by high-fluence low-power laser irradiation using fluorescence imaging techniques. *J Biomed Opt* **12**, 064015.
6 Wu S, Xing D, Gao X & Chen WR (2009) High fluence low-power laser irradiation induces mitochondrial permeability transition mediated by reactive oxygen species. *J Cell Physiol* **218**, 603–611.
7 Levy DE & Lee C-k (2002) What does Stat3 do? *J Clin Invest* **109**, 1143–1148.
8 Herrmann A, Vogt M, Monnigmann M, Clahsen T, Sommer U, Haan S, Poli V, Heinrich PC & Muller-Newen G (2007) Nucleocytoplasmic shuttling of

persistently activated STAT3. *J Cell Sci* **120**, 3249–3261.
9 Bromberg J & Darnell JE Jr (2000) The role of STATs in transcriptional control and their impact on cellular function. *Oncogene* **19**, 2468–2473.
10 Jou MJ, Jou SB, Chen HM, Lin CH & Peng TI (2002) Critical role of mitochondrial reactive oxygen species formation in visible laser irradiation-induced apoptosis in rat brain astrocytes (RBA-1). *J Biomed Sci* **9**, 507–516.
11 Matsui S, Tsujimoto Y & Matsushima K (2007) Stimulatory effects of hydroxyl radical generation by Ga–Al–As laser irradiation on mineralization ability of human dental pulp cells. *Biol Pharm Bull* **30**, 27–31.
12 Allen RG & Tresini M (2000) Oxidative stress and gene regulation. *Free Radic Biol Med* **28**, 463–499.
13 Simon AR, Rai U, Fanburg BL & Cochran BH (1998) Activation of the JAK–STAT pathway by reactive oxygen species. *Am J Physiol* **275**, C1640–C1652.
14 Lo RK, Cheung H & Wong YH (2003) Constitutively active Galpha16 stimulates STAT3 via a c-Src/JAK- and ERK-dependent mechanism. *J Biol Chem* **278**, 52154–52165.
15 Liu T, Castro S, Brasier AR, Jamaluddin M, Garofalo RP & Casola A (2004) Reactive oxygen species mediate virus-induced STAT activation: role of tyrosine phosphatases. *J Biol Chem* **279**, 2461–2469.
16 Zhang J, Xing D & Gao X (2008) Low-power laser irradiation activates Src tyrosine kinase through reactive oxygen species-mediated signaling pathway. *J Cell Physiol* **217**, 518–528.
17 Sharman WM, Allen CM & van Lier JE (1999) Photodynamic therapeutics: basic principles and clinical applications. *Drug Discov Today* **4**, 507–517.
18 Wang Y, Botvinick EL, Zhao Y, Berns MW, Usami S, Tsien RY & Chien S (2005) Visualizing the mechanical activation of Src. *Nature* **434**, 1040–1045.
19 Shvartsman DE, Donaldson JC, Diaz B, Gutman O, Martin GS & Henis YI (2007) Src kinase activity and SH2 domain regulate the dynamics of Src association with lipid and protein targets. *J Cell Biol* **178**, 675–686.
20 Yu H & Jove R (2004) The STATs of cancer – new molecular targets come of age. *Nat Rev Cancer* **4**, 97–105.
21 Masuda M, Suzui M, Yasumatu R, Nakashima T, Kuratomi Y, Azuma K, Tomita K, Komiyama S & Weinstein IB (2002) Constitutive activation of signal transducers and activators of transcription 3 correlates with cyclin D1 overexpression and may provide a novel prognostic marker in head and neck squamous cell carcinoma. *Cancer Res* **62**, 3351–3355.
22 Wang JM, Chao JR, Chen W, Kuo ML, Yen JJ & Yang-Yen HF (1999) The antiapoptotic gene mcl-1 is up-regulated by the phosphatidylinositol 3-kinase/Akt signaling pathway through a transcription factor complex containing CREB. *Mol Cell Biol* **19**, 6195–6206.
23 Youle RJ & Strasser A (2008) The BCL-2 protein family: opposing activities that mediate cell death. *Nat Rev Mol Cell Biol* **9**, 47–59.
24 Kanda N, Seno H, Konda Y, Marusawa H, Kanai M, Nakajima T, Kawashima T, Nanakin A, Sawabu T, Uenoyama Y *et al.* (2004) STAT3 is constitutively activated and supports cell survival in association with survivin expression in gastric cancer cells. *Oncogene* **23**, 4921–4929.
25 Aoki Y, Feldman GM & Tosato G (2003) Inhibition of STAT3 signaling induces apoptosis and decreases survivin expression in primary effusion lymphoma. *Blood* **101**, 1535–1542.
26 Bowman T, Broome MA, Sinibaldi D, Wharton W, Pledger WJ, Sedivy JM, Irby R, Yeatman T, Courtneidge SA & Jove R (2001) Stat3-mediated Myc expression is required for Src transformation and PDGF-induced mitogenesis. *Proc Natl Acad Sci USA* **98**, 7319–7324.
27 Lavi R, Shainberg A, Friedmann H, Shneyvays V, Rickover O, Eichler M, Kaplan D & Lubart R (2003) Low energy visible light induces reactive oxygen species generation and stimulates an increase of intracellular calcium concentration in cardiac cells. *J Biol Chem* **278**, 40917–40922.
28 Giannoni E, Buricchi F, Raugei G, Ramponi G & Chiarugi P (2005) Intracellular reactive oxygen species activate Src tyrosine kinase during cell adhesion and anchorage-dependent cell growth. *Mol Cell Biol* **25**, 6391–6403.
29 Chiarugi P & Cirri P (2003) Redox regulation of protein tyrosine phosphatases during receptor tyrosine kinase signal transduction. *Trends Biochem Sci* **28**, 509–514.
30 Reth M (2002) Hydrogen peroxide as second messenger in lymphocyte activation. *Nat Immunol* **3**, 1129–1134.
31 Reth M & Brummer T (2004) Feedback regulation of lymphocyte signalling. *Nat Rev Immunol* **4**, 269–277.
32 Singh DK, Kumar D, Siddiqui Z, Basu SK, Kumar V & Rao KV (2005) The strength of receptor signaling is centrally controlled through a cooperative loop between Ca^{2+} and an oxidant signal. *Cell* **121**, 281–293.
33 Kruman I, Guo Q & Mattson MP (1998) Calcium and reactive oxygen species mediate staurosporine-induced mitochondrial dysfunction and apoptosis in PC12 cells. *J Neurosci Res* **51**, 293–308.
34 Woetmann A, Nielsen M, Christensen ST, Brockdorff J, Kaltoft K, Engel AM, Skov S, Brender C, Geisler C, Svejgaard A *et al.* (1999) Inhibition of protein phosphatase 2A induces serine/threonine phosphorylation, subcellular redistribution, and functional inhibition of STAT3. *Proc Natl Acad Sci USA* **96**, 10620–10625.
35 Fisher SA, Langille BL & Srivastava D (2000) Apoptosis during cardiovascular development. *Circ Res* **87**, 856–864.

36 Ferreira CG, Epping M, Kruyt FA & Giaccone G (2002) Apoptosis: target of cancer therapy. *Clin Cancer Res* **8**, 2024–2034.
37 Perrimon N & McMahon AP (1999) Negative feedback mechanisms and their roles during pattern formation. *Cell* **97**, 13–16.
38 Zhang L, Gao L, Zhao L, Guo B, Ji K, Tian Y, Wang J, Yu H, Hu J, Kalvakolanu DV *et al*. (2007) Intratumoral delivery and suppression of prostate tumor growth by attenuated Salmonella enterica serovar typhimurium carrying plasmid-based small interfering RNAs. *Cancer Res* **67**, 5859–5864.